X-ray study of structural modulations in Cs_2HgCl_4

2000 J. Phys.: Condens. Matter 12 8111

(http://iopscience.iop.org/0953-8984/12/37/310)

J. Phys.: Condens. Matter **12** (2000) 8111–8125. Printed in the UK PII: S0953-8984(00)14086-X

X-ray study of structural modulations in Cs_2HgCl_4

Bagautdin Bagautdinov† and I David Brown

Brockhouse Institute of Materials Research, McMaster University, Hamilton, Ontario L8S 4M1, Canada

E-mail: bagautdi@sci.himeji-tech.ac.jp

Received 22 May 2000, in final form 4 August 2000

Abstract. High resolution x-ray diffraction at temperatures from 7 to 300 K shows that at room temperature caesium tetrachloromercurate Cs_2HgCl_4 has the β-K_2SO_4 structure but on cooling exhibits a sequence of incommensurate and commensurate modulations along $\boldsymbol{a}^*$ and $\boldsymbol{c}^*$ axes. Two modulation phases, one of which is incommensurate, are found between 184 and 221 K with wavevectors along $\boldsymbol{a}^*$ and, below 184 K, six further modulation phases, one of which is incommensurate, are found with wavevectors along $\boldsymbol{c}^*$.

1. Introduction

Caesium tetrachloromercurate, Cs_2HgCl_4, belongs to the A_2BX_4 (A = K, Rb, Cs, . . .; B = S, Se, Zn, Hg,. . .; X = O, Cl, Br,. . .) family of compounds and, like many of them, is expected to show modulated distortions, including incommensurate phases, at lower temperatures. At least eight phase transitions have been previously observed in Cs_2HgCl_4 crystals at temperatures $T_1 = 221$ K, $T_2 = 195$ K, $T_3 = 184$ K, $T_4 = 175$ K, $T_5 = 172$ K, $T_6 = 169$ K, $T_7 = 163$ K, $T_8 = 112$ K in dielectric studies by Dmitriev *et al* (1988) and Kallaev *et al* (1990a), Raman light scattering by Dmitriev *et al* (1988), NQR by Boguslavskii *et al* (1985), heat capacity measurements by Petrov *et al* (1988) and optical birefringence and ultrasonic measurements by Vlokh *et al* (1990) as illustrated in figure 1. In particular, the anomalies of dielectric permittivity (Kallaev *et al* 1990a) and NQR (Boguslavskii *et al* 1985) that occur at T_1 are similar to those seen at the normal–incommensurate transition in other incommensurate A_2BX_4 compounds.

At high temperatures many crystals of the family A_2BX_4 are isomorphous with β-K_2SO_4 (space group $Pnma$, $Z = 4$) in which all atoms, except two X atoms of the BX_4 tetrahedral anion, lie on the crystallographic mirror plane. However in most of these compounds it is believed that the mirror plane is only statistically present and that locally the atoms are displaced to one side or the other by rotations of the tetrahedral BX_4 groups about the $\boldsymbol{a}$ and $\boldsymbol{c}$ axes. On lowering the temperature the displacements order to form a modulated wave. The experimental results point to an order–disorder mechanism for the modulation (de Pater *et al* 1979, Itoh *et al* 1983), except in K_2SeO_4 where Iizumi *et al* (1977) found clear evidence of a soft mode.

In spite of several structural investigations of Cs_2HgCl_4, the nature of the rich collection of low temperature phases is poorly understood. We have therefore carried out an x-ray study in the range 7–300 K, which confirms the existence of both incommensurate and commensurate modulated phases that occur as modulation waves directed along both the $\boldsymbol{a}$ and $\boldsymbol{c}$ axes.

† Present address: Himeji Institute of Technology, Department of Life Science, 3-2-1 Koto, Kamigori-cho, Ako-gun, Hyogo 678-1297, Japan.

0953-8984/00/378111+15$30.00

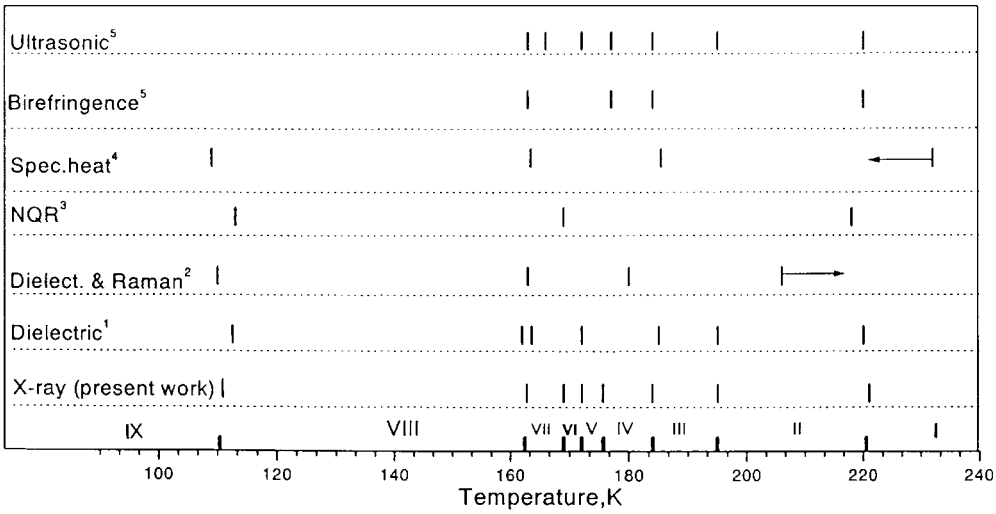

Figure 1. Phase transition sequences of Cs_2HgCl_4. 1, Kallaev *et al* (1990a); 2, Dmitriev *et al* (1988); 3, Boguslavskii *et al* (1985); 4, Petrov *et al* (1988); 5, Vlokh *et al* (1990). The x-ray results are from the present work.

2. Experimental details

Measurement of a complete set of intensities at room temperature on a Siemens R3m/V diffractometer (Mo Kα radiation) with a spherical specimen of diameter 0.2 mm gave lattice parameters of $a_0 = 9.770(2)$, $b_0 = 7.572(2)$ and $c_0 = 13.355(3)$ Å corresponding to the *Pnma* setting of space group No 62 (Hahn 1983). These measurements were used to confirm that Cs_2HgCl_4 has the β-K_2SO_4 structure at room temperature.

The x-ray experiments at other temperatures were carried out on a high resolution four-circle Huber goniometer with 18 kW rotating anode x-ray tube (Cu Kα radiation) using the (002) plane of a pyrolytic graphite crystal as monochromator. The diffractometer was equipped with a closed cycle He refrigerator capable of operating between 7 and 300 K with an accuracy of ± 0.005 K. The plate shaped specimen with approximate dimension $2.5 \times 2.0 \times 1.0$ mm^3 was mounted in reflecting geometry on the cold finger of the refrigerator in the presence of He exchange gas inside a beryllium heat shield. The software permitted q-scans around Bragg and satellite reflections in the hardware limited range $2\theta = 0$–80°.

3. Experimental results and discussion

3.1. Sequence of phases

Our measurements show that Cs_2HgCl_4 has a complex phase diagram in which some phases can coexist depending on the thermal history of the crystal. Nine phases have been identified, labelled in order of decreasing temperature as A, B, C, D, E, F, G, H and I. Phase A is the high temperature disordered form with the *Pnma* β-K_2SO_4 structure, phases B and C show modulation along the $\boldsymbol{a}^*$ axis and phases D to I show modulation along the $\boldsymbol{c}^*$ axis. The modulations of phases B and F are incommensurate.

3.1.1. Phase A (high temperature, Pnma, $a = a_0$, $b = b_0$, $c = c_0$, exists above $T_1 = 221$ K). The structure at room temperature has been reported as both centrosymmetric, *Pnma* (Linde

et al 1983), which is the space group for other observed β-K_2SO_4 structures, and later by Pakhomov *et al* (1992a) as non-centrosymmetric, $P2_12_12_1$, on the grounds that the crystal showed a non-zero piezoelectric coefficient (Pakhomov *et al* 1992b) and some of the systematic absences of $Pnma$ appeared to be violated though the authors give few details. In any case the differences between the reported structures, apart from the different space groups used, are not significant and both agree with our determination of the structure at room temperature. Above T_1 (temperature range I in figure 1) we found no violation of the systematic absence ($hk0$: $h = 2n + 1$, $0kl$: $k + l = 2n + 1$) indicating the space group is $Pnma$ or $Pn2_1a$. We assumed the space group $Pnma$ since this is the space group reported for the high temperature phase of β-K_2SO_4.

3.1.2. Phase B (incommensurate, $Pnma(\alpha, 0, 0)0ss$, $\boldsymbol{q} = (\frac{4}{5} - \delta)\boldsymbol{a}_0^*$, $a \sim 5a_0$, $b = b_0$, $c = c_0$. Observed between $T_1 = 221$ K and $T_3 = 184$ K). Below T_1 (221 K) satellite reflections appear at positions near $\frac{4}{5}\boldsymbol{a}_0^*$ on each side of the systematically allowed $hk0$: $h = 2n$ Bragg reflections (or, alternatively, at $\frac{1}{5}\boldsymbol{a}_0^*$ on each side of the absent h odd reflections) as shown in figure 2. Since the satellites are incommensurate with the main diffraction pattern and their positions vary with temperature, it is convenient to describe their wavevector as $\boldsymbol{q} = (\frac{4}{5} - \delta)\boldsymbol{a}_0^*$ with δ varying from 0.045 at T_1 to 0.0 where the lock-in phase C appears at T_3 (184 K). Satellites were observed in the ($hk0$) layer but not along $h00$ or in the ($h0l$) and ($0kl$) layers. Apart from the presence of the satellites, the diffraction pattern remains the same as in phase A. The presence of only first order satellites along [100] indicates a sinusoidally modulated structure with the wavevector parallel to $\boldsymbol{a}_0^*$. This behaviour is similar to that seen in the incommensurate modulated phases of K_2SeO_4 (Iizumi *et al* 1977) where the wavevector is $(\frac{2}{3} + \delta)\boldsymbol{a}_0^*$, implying that the atomic modulations in Cs_2HgCl_4 are also likely to involve rotations of the tetrahedral groups around the $\boldsymbol{a}$ and $\boldsymbol{c}$ axes consistent with the observed satellite reflections.

The positions of the satellite at $(\frac{4}{5} - \delta)\boldsymbol{a}_0^*$ on either side of the observed Bragg reflection indicates that the wavelength of the modulation in real space is close to $\frac{5}{4}a_0$, the modulation completing about four wavelengths in the distance of $5a_0$ lattice spacing. The extinction condition for these satellites is $hk0m$: $h + m =$ odd, corresponding to the superspace group $Pnma(\alpha, 0, 0)0ss$ (Janssen *et al* 1993). The second extinction rule for satellites of this group, $h0lm$: $m =$ odd, is automatically satisfied by the absence of $h0lm$ satellites.

The temperature dependence of the modulation wavevector on both cooling and heating is shown in figure 3(a). As the temperature is lowered, the position of the satellite varies continuously from about $\boldsymbol{q} = \frac{3}{4}\boldsymbol{a}_0^*$ ($\delta = 0.045$) at T_1 (221 K) to $\boldsymbol{q} = \frac{4}{5}\boldsymbol{a}_0^*$ ($\delta = 0$) just below T_3 (184 K), the continuous variation with temperature providing further evidence that the modulation is incommensurate. Figure 3(b) shows that the intensity of the $(\frac{4}{5} - \delta, 6, 0)$ satellite reflection increases monotonically as the temperature is lowered, while its width, shown in figure 3(c), decreases rapidly with temperature, becoming resolution limited below 210 K. The positions of the satellites show hysteresis: on heating, phase B does not appear until T_2 (195 K), but the changes in width and intensity are reversible.

3.1.3. Phase C (commensurate, $Pn2_1a$, $\boldsymbol{q} = \frac{4}{5}\boldsymbol{a}_0^*$, $a = 5a_0$, $b = b_0$, $c = c_0$. Observed between $T_2 = 195$ K and $T_3 = 184$ K). In this phase, which is essentially only observed on heating, the satellite reflections lock in at $\boldsymbol{q} = \frac{4}{5}\boldsymbol{a}_0^*$. Because all $hk0$ reflections with h odd are missing (indexed on the supercell), the crystal possesses an a-glide plane. The diffraction pattern of the ($h0l$) and ($0kl$) layers is the same as in phases A and B. Hence, the space group of phase C is $Pnma$ or $Pn2_1a$. The observation of a spontaneous $\boldsymbol{b}$ axis polarization between T_2 and T_3 by Kallaev *et al* (1990a) requires the non-centrosymmetric space group $Pn2_1a$, with

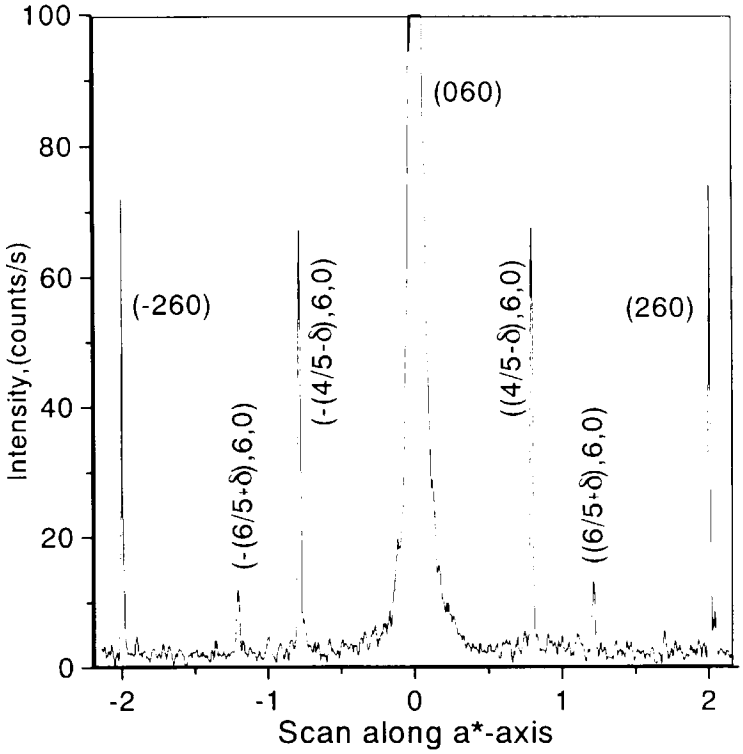

Figure 2. X-ray scattering patterns of the $h60$ reflections of the incommensurate phase B at 200 K.

the loss of the mirror plane. In this phase, the supercell is composed of five cells of phase A and all atoms are located on general positions.

Pakhomov *et al* (1992b) report a unit cell at 190 K with the space group $P2_1$ and the lattice parameters of the subcell. They apparently failed to notice any superlattice reflections in their sample which they examined using a four-circle diffractometer.

3.1.4. Phase D (commensurate, $P112_1/a$, $\boldsymbol{q} = \frac{1}{3}\boldsymbol{c}_0^*$, $a = a_0$, $b = b_0$, $c = 3c_0$. Observed between $T_3 = 184$ K and $T_4 = 175$ K). Observations in the $(0kl)$ and $(h0l)$ planes show that below T_3 satellites appear along the $\boldsymbol{c}^*$ direction. The satellite reflections at $(0, k, l \pm \frac{1}{3})$, indicating the presence of a new phase D in temperature range 184–175 K (figures 4(a), 5(a)), do not change position with temperature confirming that this is a commensurate phase. The reflection conditions in the three-cell superstructure are: $hk0$: $h = 2n$, $00l$: $l = 2n$, $h00$: $h = 2n$ indicating the centrosymmetric space group $P112_1/a$.

3.1.5. Phase E (commensurate, $P2_1/n11$, $\boldsymbol{q} = \frac{2}{5}\boldsymbol{c}_0^*$, $a = a_0$, $b = b_0$, $c = 5c_0$. Observed between $T_4 = 175$ K and $T_5 = 172$ K). Below $T_4 = 175$ K the $\boldsymbol{c}^*$ axis satellites in the $(0kl)$ plane jump from $\boldsymbol{q} = \frac{1}{3}\boldsymbol{c}_0^*$ to $\frac{2}{5}\boldsymbol{c}_0^*$ and stay at this position down to T_5 (figure 4(b)). In the $(h0l)$ plane the satellites appear at $\frac{1}{5}\boldsymbol{c}_0^*$ on each side of the observed reflections (figure 5(b)). Phase E (175–172 K) has the reflection conditions in the five-cell superstructure: $0kl$: $k + l = 2n$, $h00$: $h = 2n$, $0k0$: $k = 2n$, $00l$: $l = 2n$ corresponding to the space group $P2_1/n11$, with a modulation of two wavelengths along the $\boldsymbol{c}$ axis.

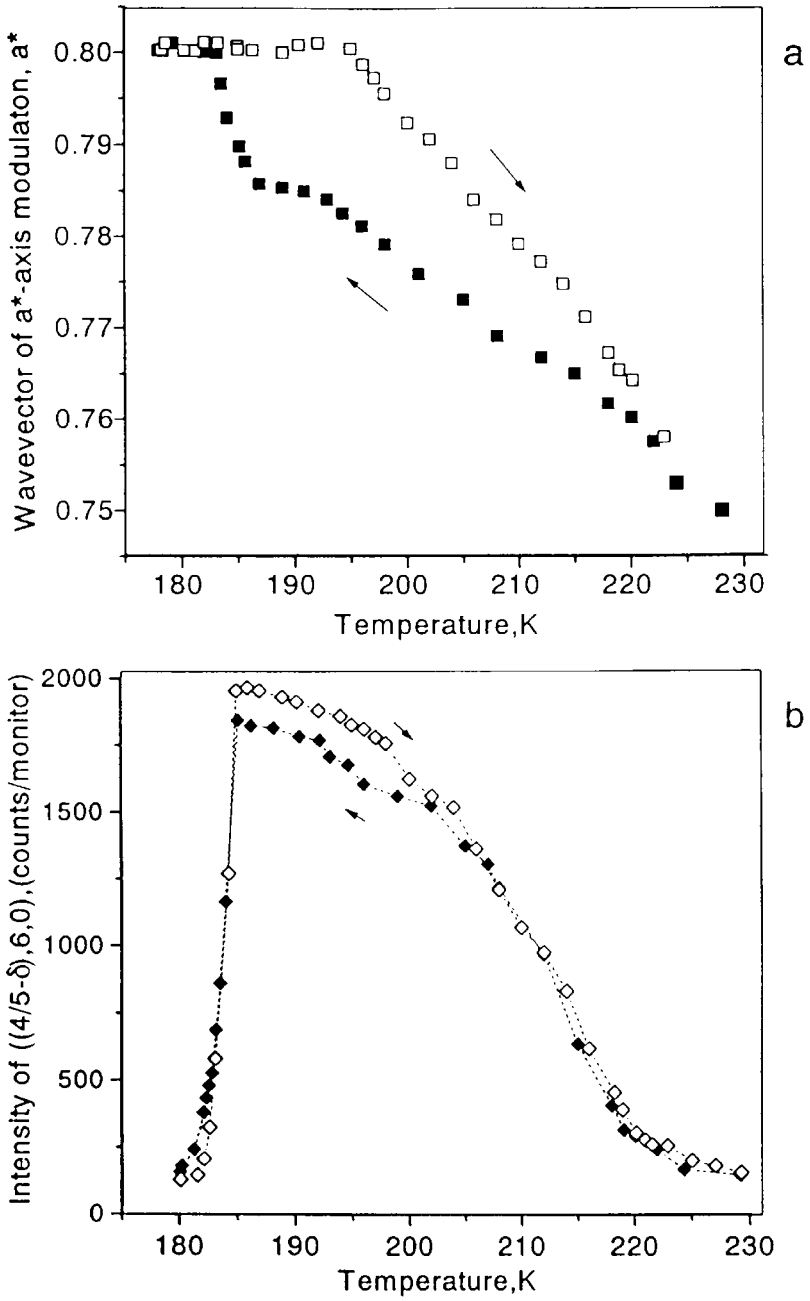

Figure 3. The temperature dependences (a) of the modulation wavevector $\boldsymbol{q} = (\frac{4}{5} - \delta)\boldsymbol{a}_0^*$, (b) of the intensity of the satellite reflection at $(\frac{4}{5} - \delta, 6, 0)$ and (c) of the satellite peak full width at half maximum (FWHM).

3.1.6. Phase F (incommensurate, $\boldsymbol{q} = (\frac{3}{7} - \delta)\boldsymbol{c}_0^*$, $a = a_0$, $b = b_0$, $c \sim 7c_0$. Observed between $T_5 = 172$ K and $T_6 = 169$ K). Phase F is characterized by satellites in the plane $(0kl)$ corresponding to a modulation wavevector that changes from $\frac{2}{5}\boldsymbol{c}_0^*$ to $\frac{3}{7}\boldsymbol{c}_0^*$ as the temperature

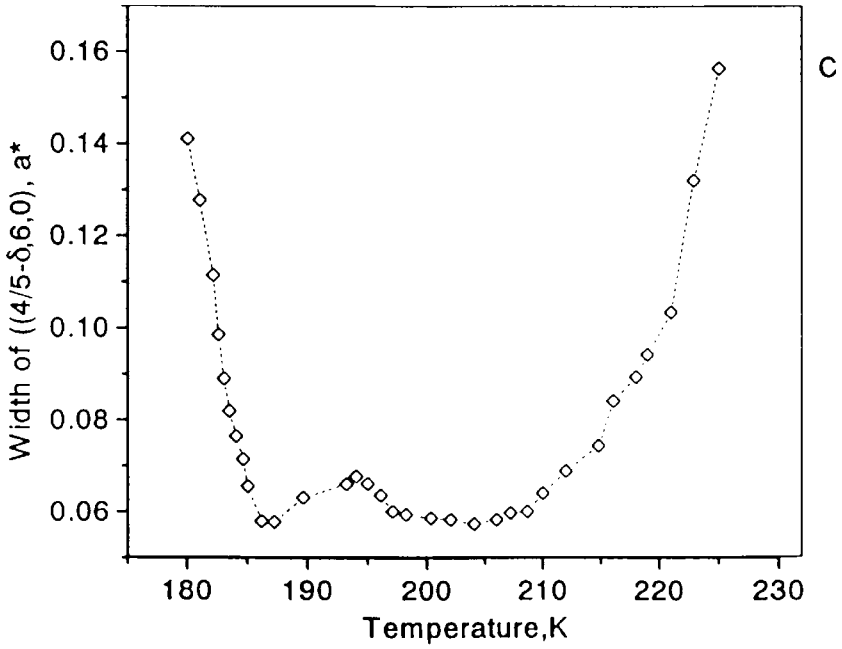

Figure 3. (Continued)

is lowered. The wavevector can be described as $\boldsymbol{q} = (\frac{3}{7} - \delta)\boldsymbol{c}_0^*$ measured from the observed reflections. In the $(h0l)$ plane the satellites appear at between $\frac{1}{5}\boldsymbol{c}_0^*$ and $\frac{1}{7}\boldsymbol{c}_0^*$ from the observed reflections. The temperature dependence of the position of the satellites indicates that the modulation is incommensurate.

3.1.7. Phase G (commensurate, $P2_12_12_1$, $\boldsymbol{q} = \frac{3}{7}\boldsymbol{c}_0^*$, $a = a_0$, $b = b_0$, $c = 7c_0$. Observed between $T_6 = 169$ K and $T_7 = 163$ K). Satellite reflections in the $(0kl)$ plane lock into the position $\frac{3}{7}\boldsymbol{c}_0^*$ (figure 4(c)) relative to the observed reflections. In the $(h0l)$ plane the satellites occur $\frac{1}{7}\boldsymbol{c}_0^*$ from the observed reflections (figure 5(c)). The reflection conditions in the seven-cell superstructure are: $h00$: $h = 2n$, $0k0$: $k = 2n$ $00l$: $l = 2n$ indicating the polar space group, $P2_12_12_1$. As expected for a non-centrosymmetric structure, this phase has a large dielectric constant and piezoelectric coefficient (Kallaev *et al* 1990b).

A structure for Cs_2HgCl_4 at 170 K with $c = 2c_0$ was reported in the space group $P1$ by Pakhomov *et al* (1992b). It is not clear whether they examined the F or G phase but in either case they missed the modulation reflection at $l_0 = \frac{1}{7}$ and mistook the modulation reflection at $l_0 = \frac{3}{7}$ for a commensurate superstructure reflection at $l_0 = \frac{1}{2}$. There are other problems with their refinement. The $HgCl_4^{2-}$ ions show large unexpected (and unexplained) distortions with bond valence sums around Hg ranging from 2.2 to 2.9 valence units (vu). Deviations of more than 0.3 vu from the expected value of 2.0 are usually indicative of an incorrect structure.

3.1.8. Phase H (commensurate, $P12_1/c1$, $\boldsymbol{q} = \frac{1}{2}\boldsymbol{c}_0^*$, $a = a_0$, $b = b_0$, $c = 2c_0$. Observed between $T_7 = 163$ K and $T_8 = 112$ K). On cooling below $T_6 = 163$ K the satellites at $\frac{3}{7}\boldsymbol{c}_0^*$ in the $(0kl)$ plane are replaced by satellites at $\frac{1}{2}\boldsymbol{c}_0^*$ (figure 4(d)) and their position remains unchanged down to at least 7 K. In the $(h0l)$ plane the satellites abruptly disappear but the

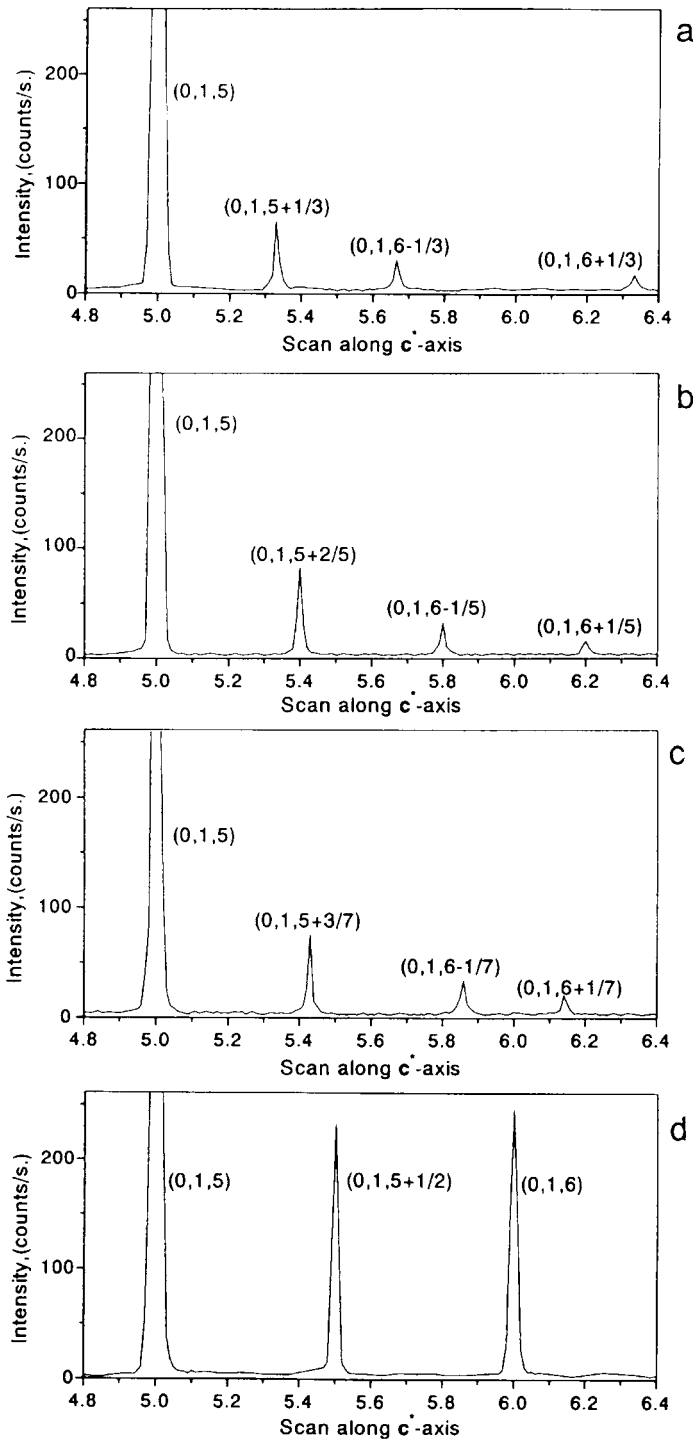

Figure 4. Evolution of the x-ray scattering patterns of the 0*kl* reflections scanned along the c^* direction at temperatures: (a) 177 K (phase D), (b) 174 K (phase E), (c) 167 K (phase G), (d) 150 K (phase H).

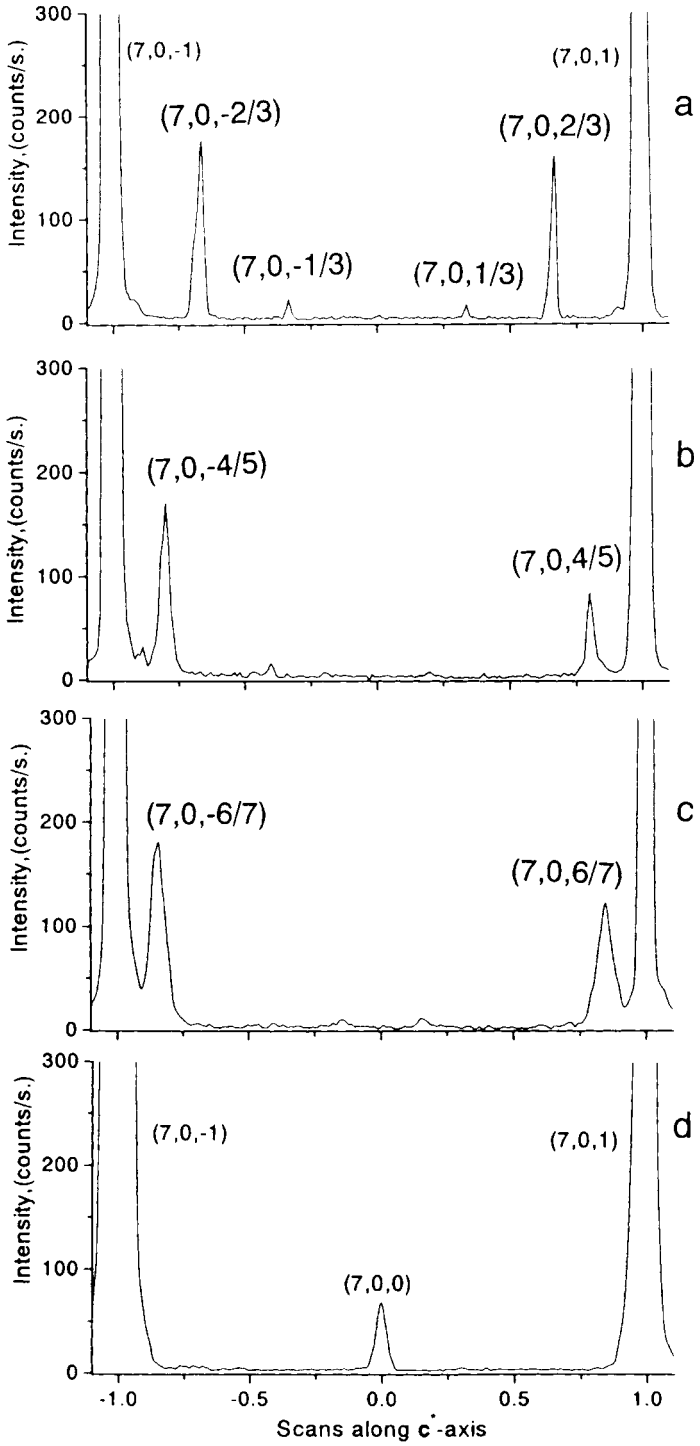

Figure 5. Evolution of the x-ray scattering patterns of the $h0l$ reflections scanned along the c_0^* direction at temperatures: (a) 177 K (phase D), (b) 174 K (phase E), (c) 167 K (phase G), (d) 150 K (phase H).

$h00$: $h = 2n + 1$ reflections that were systematically absent in the $Pnma$ A phase now appear (figure 5(d)). The reflection conditions for the doubled c-cell observed in the temperature range 163–112 K are: $h0l$: $l = 2n$, $0k0$: $k = 2n$, $00l$: $l = 2n$ corresponding to space group $P12_1/c1$.

3.1.9. Phase I (commensurate, $P1c1$, $\boldsymbol{q} = \frac{1}{2}\boldsymbol{c}_0^*$, $a = a_0$, $b = b_0$, $c = 2c_0$. Observed below $T_8 = 112$ K). Around $T_8 = 112$ K our x-ray measurements do not detect any change of wavevector, but a transition is suggested by the appearance of weak Bragg reflections at $0k0$: $k = 2n + 1$, indicating that the 2_1 axis is lost. The possible space groups corresponding to the reflection conditions: $h0l$: $l = 2n$, $00l$: $l = 2n$ are $P12/c1$ or $P1c1$ but $P12/c1$ can be ruled out as it is not compatible with the arrangement of the tetrahedral ions.

3.2. Temperature behaviour

The behaviour of Cs_2HgCl_4 on cooling is different from its behaviour on heating. On cooling phase A from room temperature, weak diffuse peaks appear close to the positions of the phase B satellites at about 15 K above T_1, characteristic of a pretransitional modulated state with a short correlation length. The intensity of the diffuse scattering increases as the temperature is lowered until at T_1 it transforms into recognizable satellite peaks. The value of T_1, 221 K, is determined by the linear extrapolation of the intensity of the B phase ($\frac{4}{5} - \delta$, 6, 0) satellite shown in figure 3(b). This value coincides with the dielectric anomaly at 220.5 K reported by Kallaev *et al* (1990a) and the acoustic anomaly at 220 K reported by Vlokh *et al* (1990). In the region of T_1 the temperature dependence of the intensities and positions of the satellites are the same on both heating and cooling, consistent with a second order phase transition. The intensity of the satellites does not vary with time when the temperature is held constant, showing that the modulated structure is stable. On lowering the temperature, the intensity strongly increases to a maximum at a temperature around 185 K indicating a continuous increase in the proportion of the sample showing modulation ordering (figure 3(b)). The satellites also become narrower as the temperature is reduced below T_1 reaching the resolution limit around 211 K (figure 3(c)). Close to 184 K the B phase rapidly collapses. The intensity drops, the peak broadens and the wavevector increases from $0.786\boldsymbol{a}_0^*$ to the commensurate value of $0.8\boldsymbol{a}_0^*$ characteristic of phase C.

The process is not reversible. On heating, phase C remains stable until T_2 (195 K) at which point the modulation becomes unlocked and the satellites start shifting to lower wavenumber, consistent with a continuous transition to phase B (figure 3(a)). Thus, the $\boldsymbol{a}^*$ modulation wavevector shows a large thermal hysteresis over the temperature range T_1 to T_3 (figure 3(a)). A similar thermal hysteresis is observed even when the heating and cooling are cycled at temperatures between T_1 and T_2. Such thermal hysteresis indicates a first order transition with defects pinning the modulation wave and preventing the crystal from reaching thermal equilibrium. Phase C occurs between T_2 and T_3 only during heating; on cooling it is observed only between 184 and 181 K where it coexists with phase D.

This behaviour is consistent with the mirror plane of the A phase being only statistically present. The phase is disordered with local violation of the mirror symmetry but with little coherence of the distortions from one cell to the next. As the temperature drops below 235 K, small regions of coherent modulation with a wavevector close to $0.75\boldsymbol{a}_0$ appear fleetingly but it is not until a temperature of 221 K that the modulations become stable, coinciding with a broad peak in the specific heat (Petrov *et al* 1988), and anomalies in the dielectric constant (Kallaev *et al* 1990a) and the velocities of ultrasonic waves (Kityk *et al* 1992). The stable structure at 221 K has modulations with a correlation length of 50 Å but with most of the

crystal remaining disordered. As the temperature is lowered to 211 K, the modulated regions grow rapidly in size to over 200 Å and occupy about half the crystal, the other half still being disordered. At the same time, the modulation wavevector increases until at T_3 (184 K) the B phase rapidly collapses to the commensurate phase C with a wavevector of $0.8\boldsymbol{a}_0^*$. On heating, phase C remains stable to T_2 (195 K).

At 184 K a major transition occurs as the direction of the modulation wavevector changes from $\boldsymbol{a}^*$ to $\boldsymbol{c}^*$. The transition is accompanied by sharp discontinuities in the specific heat (Petrov *et al* 1988) and the velocity of ultrasound waves (Kityk *et al* 1992), and it sometimes results in the disintegration of the crystal suggesting that it involves considerable stress. In the P–T phase diagram given by Kityk *et al* (1992) the temperature of this transition drops with increasing pressure in contrast to most of the other transitions which have large positive values of $\mathrm{d}T/\mathrm{d}P$. Below 182 K the phases B and C disappear completely, and the compound shows a devil's staircase of commensurate and incommensurate modulations parallel to $\boldsymbol{c}^*$ down to the lowest temperatures studied (7 K) (phases D to I). Initially, the modulation wavevector is $\frac{1}{3}\boldsymbol{c}_0^*$ (phase D). At 175 K it jumps to $\frac{2}{5}\boldsymbol{c}_0^*$ (phase E). Between 172 and 169 K the modulation becomes unlocked and increases smoothly from $\frac{2}{5}\boldsymbol{c}_0^*$ to $\frac{3}{7}\boldsymbol{c}_0^*$ (phase F) where it again locks in (phase G). However, the incommensurate phase F shows hysteresis with phase E remaining below 172 K on cooling and phase G remaining above 169 K on heating. At 163 K the modulation wavevector increases again to $\frac{1}{2}\boldsymbol{c}_0^*$ (phase H). The lowest phase transition at 112 K does not involve a change in wavevector, only a change in the extinction condition with the loss of the twofold screw axis.

The hysteresis behaviour and discontinuities in the wavevectors (figures 3(a), 6) and the lattice parameters (figure 7) indicate that the transitions from B to C at 195 K, C to D at 184 K, D to E at 175 K, F to G at 169 K and G to H at 163 K are first order. This last transition is particularly abrupt with a sharp peak in the specific heat (Petrov *et al* 1988), a reversal in the piezoelectric coefficient (Kallaev *et al* 1990b) and an increase in the number of lines found in the ^{35}Cl NQR spectrum (Petrov *et al* 1983), consistent with the space group of H not being a subgroup of $Pnma$.

The scans along the $\boldsymbol{c}^*$ axis shown in figures 4, 5 and the temperature dependence of $\boldsymbol{q} = \gamma\boldsymbol{c}_0^*$ shown in figure 6 were obtained on cooling. On heating, the behaviour is more complex as different phases coexist. As in many modulated crystals the behaviour of the phase transitions in Cs_2HgCl_4 is sensitive to the history of the sample, the dynamic character of the measurement and whether the measurements were made during cooling or heating. The discrepancies in the reported phase transitions shown in figure 1 are likely attributable to these effects and to the lack of sensitivity of some of the experimental techniques used.

3.3. c axis modulation

The unusual feature of the present crystal is the initial modulation along the $\boldsymbol{a}$ axis, followed by a sequence of different modulations along the $\boldsymbol{c}$ axis. The $\boldsymbol{a}$ axis modulations are similar to those found in many other crystals of the β-K_2SO_4 type, but the $\boldsymbol{c}$ axis modulations appear to be unique to Cs_2HgCl_4 and deserve special consideration. They are characterized by a modulation wavelength that, over a small temperature range of 20 K, drops from $3c_0$ to $2c_0$ through a sequence of structures that follows a devil's staircase with wavelengths:

$$\lambda = (2n + 1)c_0/n \qquad \text{where } n = 1, 2 \text{ and } 3.$$

The odd number in the numerator of this expression is a consequence of the relative orientations of the tetrahedral anions in the subcell, which require that the superstructure be composed of an odd number of subcells if the modulation wave itself is to conform to the symmetry operations of a subgroup of $Pnma$.

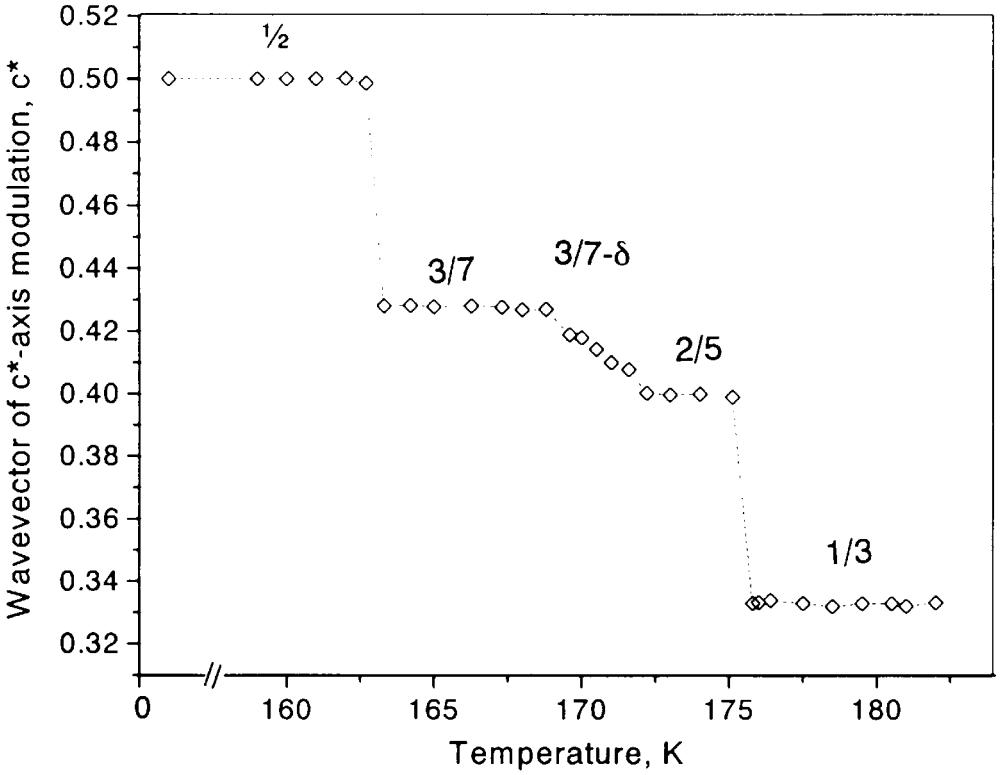

Figure 6. The temperature dependence of the modulation wavevector parallel to the c^* direction ($q = \gamma c_0^*$).

The nature of the atomic displacements of Cs_2HgCl_4 produced by the modulation wave is not known though, by comparison with other compounds in the A_2BX_4 series, they can probably be described by rotations of the $HgCl_4^{2-}$ anion with consequent displacements of the Cs^+ ions. Rotation of the anion can occur about any of the three orthogonal crystallographic directions and the effects of these rotations will be seen in the three principal planes of the diffraction pattern. Our measurements do not extend to the ($hk0$) plane, which, because it lies perpendicular to the modulation direction, contains little additional symmetry information, but it is possible to identify the nature of the rotations about [100] and [010] by looking for sequences of rotation that match the observed symmetry of the superstructure. These are summarized in table 1. When projected down either the $\boldsymbol{a}$ (figure 8(a)) or $\boldsymbol{b}$ axes (figure 8(b)) the $HgCl_4^{2-}$ anions lie approximately at the corners of a square though they occur at two different levels in the crystal. In each of the two projections the modulation can be represented by a symbolic rotation angle indicated by a signed lower case letter and these then form a $2n$ array where n depends on the modulation wavelength along the $\boldsymbol{c}$ direction (table 1). Each square of four letters refers to the square of four tetrahedral anions in the corresponding subcell shown in figure 8. Anions whose rotations are related by symmetry are assigned the same letter, and the sign associated with the letter indicates whether the rotation is clockwise or anticlockwise.

The phase angle of the modulation wave relative to the symmetry elements of the space group may be fixed, in which case table 1 gives the only possible arrangement of the displacements. If relative phases running along the two rows shown in table 1 are coupled, the symmetry relating the two rows requires that increasing the phase angle of the top row

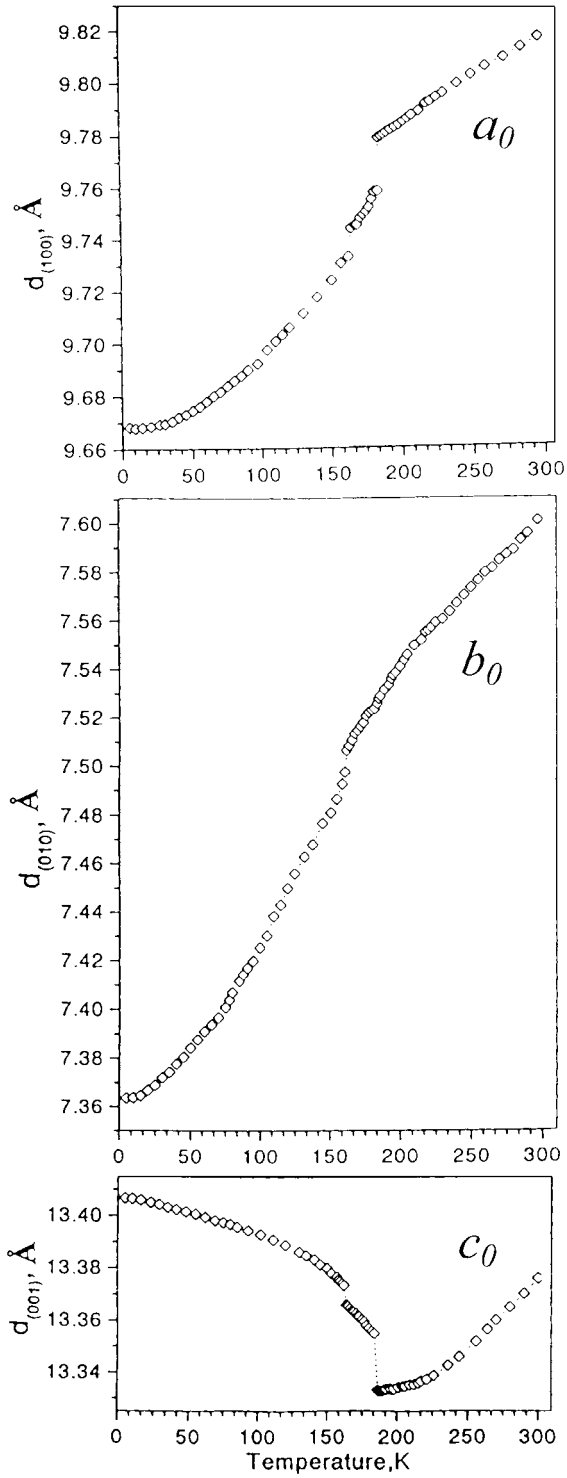

Figure 7. Lattice parameters of the subcell of Cs_2HgCl_4 as a function of temperature. The values were determined from the positions of main reflections (12, 0, 0), (0, 8, 0) and (0, 0, 16) measured in the $\theta/2\theta$ mode.

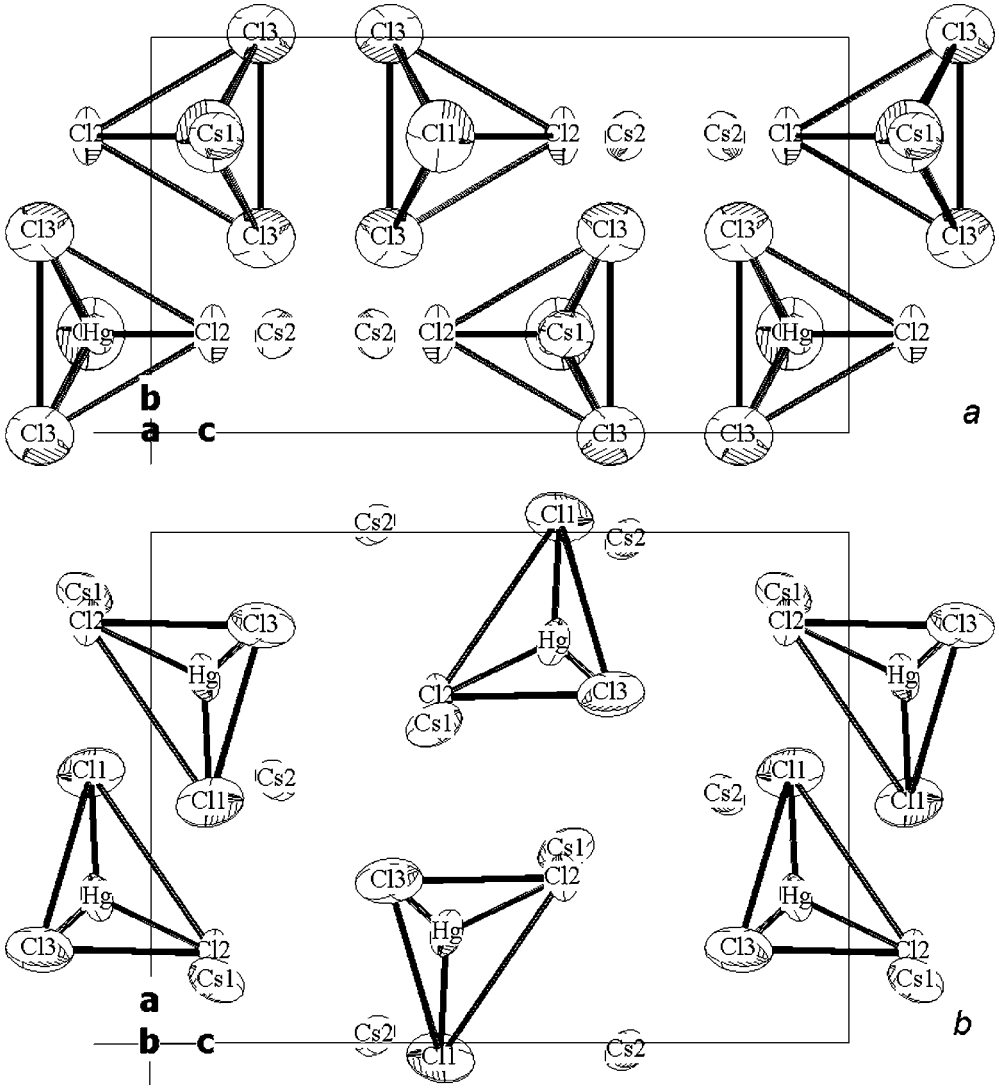

Figure 8. Projection of the structure of Cs_2HgCl_4 viewed down (a) [100], (b) [010].

decreases the phase angle of the bottom row by the same amount. If the phases are independent, symmetry specifies no relationship between them. In table 1 the undetermined phases have been arbitrarily chosen to be in phase which represents the likely consequence of a coupling between the rotations around [100] and [010].

The space groups of phases D, E and G are all subgroups of $Pnma$ in which the mirror plane is lost together with one or more of the glide planes. This is expected even though the supercell is several times larger than the subcell because the glide and screw operations relate anions that are related by the $..2_1$ operation (together with an integral number of lattice translations) of the $Pnma$ subcell. The space group of phase H, $P12_1/c1$ is not a subgroup of $Pnma$. In this phase the mirror plane and the doubling of the cell have been transformed into a glide along the modulation direction.

Table 1. Modulation patterns in the $\boldsymbol{c}$ modulated phases. The letters represent crystallographically distinct rotation angles applied to the different $HgCl_4^{2-}$ anions in the supercell, the sign indicating the direction of rotation (no sign indicates zero rotation). A centre of symmetry (if present) is chosen to lie between the first elements of the two rows. In the case of phase G, the 2_1 . . screw axis lies immediately to the right of the first element listed. See the text for an explanation of the fixed, coupled and independent phase angles of the modulation waves.

Modulation by rotation around the $\boldsymbol{a}$ axis ($\boldsymbol{b}$ axis vertical, $\boldsymbol{c}$ horizontal)	
Phase D $P112_1/a$	$+a\ +b\ -b\ -a\ -b\ +b$
(phase angles fixed)	$+a\ +b\ -b\ -a\ -b\ +b$
Phase E $P2_1/n11$	$+a\ +b\ -c\ -c\ +b\ +a\ +b\ -c\ -c\ +b$
(phase angles fixed)	$+a\ +b\ -c\ -c\ +b\ +a\ +b\ -c\ -c\ +b$
Phase G $P2_12_12_1$	$+a\ -b\ -c\ d\ +e\ +f\ -g\ -g\ +f\ +e\ d\ -c\ -b\ +a$
(phase angles fixed)	$+g\ -f\ -e\ d\ +c\ +b\ -a\ -a\ +b\ +c\ d\ -e\ -f\ +g$
Phase H $P12_1/c1$	$+a\ b\ -a\ b$
(phase angles coupled)	$+a\ b\ -a\ b$
Modulation by rotation around the $\boldsymbol{b}$ axis ($\boldsymbol{a}$ axis vertical, $\boldsymbol{c}$ horizontal)	
Phase D	$+a\ +b\ -c\ -a\ -b\ +c$
(phase angles coupled)	$+a\ +c\ -b\ -a\ -c\ +b$
Phase E	$+a\ +b\ +c\ -c\ -b\ -a\ -c\ -c\ +c\ +b$
(phase angles coupled)	$+a\ +b\ +c\ -c\ -b\ -a\ -b\ -c\ +c\ +b$
Phase G	$+a\ +b\ +c\ +d\ +e\ +f\ +g\ -a\ -b\ -c\ -d\ -e\ -f\ -g$
(phase angles coupled)	$+g\ +f\ +e\ +d\ +c\ +b\ +a\ -g\ -f\ -e\ -d\ -c\ -b\ -a$
Phase H	$+a\ -b\ +a\ -b$
(phase angles independent)	$+a\ -b\ +a\ -b$

4. Conclusions

Our analysis of the phase transitions in Cs_2HgCl_4 shows behaviour different from that shown by other crystals with the same high temperature structure. Unusually Cs_2HgCl_4 forms nine different phases including two superstructures formed by a modulation wave along the $\boldsymbol{a}$ axis and six superstructures formed by a modulation wave along the $\boldsymbol{c}$ axis.

In most compounds of the A_2BX_4 family, an incommensurate modulation first occurs along the $\boldsymbol{a}^*$ direction and with decreasing temperature locks in to a commensurate phase with a wavevector of either $0.333\boldsymbol{a}_0^*$ or $0.5\boldsymbol{a}_0^*$ though wavevectors of $0.429\boldsymbol{a}_0^*$, $0.4\boldsymbol{a}_0^*$, $\boldsymbol{a}_0^*$ are also known (Cummins 1990). Modulation along $\boldsymbol{c}^*$ has previously only been reported for the methyl ammonium and methyl phosphonium compounds $(N(CH_3)_4)_2CdI_4$, $(N(CH_3)_4)_2CuBr_4$, $(N(CH_3)_4)_2ZnI_4$ and $(P(CH_3)_4)_2CuCl_4$ (Werk *et al* 1990, Madariaga *et al* 1990), and only with the commensurate wavevector $0.5\boldsymbol{c}_0^*$.

At high temperatures the structure is disordered with the atoms apparently randomly displaced from their average positions. When the temperature drops below 236 K, the displacements become weakly coupled to form fluctuating modulation waves along the $\boldsymbol{a}$ axis with a wavelength and coherence length of around $1.3a_0$. At 221 K incommensurate modulations freeze out and by 211 K the coherent regions are over 12 wavelengths long, though even at this temperature half of the structure remains disordered. As the temperature drops further the modulation wavelength decreases until the $\boldsymbol{a}$ axis modulation collapses at 184 K, but the transition shows some hysteresis with a lock-in modulation with a wavelength of $1.25a_0$.

Below 184 K the modulation wave along the $\boldsymbol{a}$ axis is replaced by a modulation wave

along the $\boldsymbol{c}$ axis starting with a wavelength of $3c_0$ and reducing over a temperature range of 20 K through a devil's staircase of intermediate phases to $2c_0$. Below 163 K the structure remains unchanged down to 7 K except for the loss of a screw axis at 112 K. The phases we propose account for most of the phase transformations that have been observed using a variety of physical techniques ranging from electrical to mechanical measurements.

Acknowledgments

The authors are grateful to Professor B Gaulin for the use of his high resolution diffractometer, Dr Yu Yuzyuk for providing the crystals and M Lumsden for experimental help and the Natural Science and Engineering Research Council of Canada for financial support.

References

Boguslavskii A A, Lotfullin R Sh, Simonov M N, Kirilenko V V, Pakhomov V I and Mikhailova A Ya 1985 *Sov. Phys.–Solid State* **27** 321

Cummins H Z 1990 *Phys. Rep.* **185** 211

de Pater C J, Axe J D and Currat R 1979 *Phys. Rev.* B **19** 4684

de Wolff P M, Janssen T and Janner A 1981 *Acta Crystallogr.* A **37** 625

Dmitriev V P, Yuzyuk Yu I, Tregubchenko A V, Larin E S, Kirilenko V V and Pakhomov V I 1988 *Sov. Phys.–Solid State* **30** 704

Hahn T (ed) 1983 *International Table for Crystallography* vol A (Dordrecht: Kluwer) p 854

Iizumi M, Axe J D, Shirane G and Shimaoke K 1977 *Phys. Rev.* B **15** 4392

Itoh K, Hinasada A, Matsunaga H and Nakamura E 1983 *J. Phys. Soc. Japan* **52** 664

Janssen T, Janner A, Looijenga-Vos A and de Wolff P M 1993 *International Table for Crystallography* vol C, ed A J C Wilson (Dordrecht: Kluwer) ch 9.8, p 797

Kallaev S N, Gladkii V V, Kirikov V A and Kamilov I K 1990a *Ferroelectrics* **106** 299

Kallaev S N, Gladkii V V, Kirikov V A and Lipinski I E 1990b *Phase Transitions* **29** 85

Kityk A V, Soprunyuk V P, Vlokh O G, Olekseyuk I D and Piroga S A 1992 *Sov. Phys.–Solid State* **34** 2044

Linde S A, Mikhaylova A Y, Pakhomov V I, Kirilenko V V and Shulga V G 1983 *Koord. Khim.* **9** 998

Madariaga G, Albertdi M M and Zuniga F J 1990 *Acta Crystallogr.* C **46** 2363

Pakhomov V I, Goryunov A V, Ivanova-Korfini I N, Boguslavskii A A and Lotfulilin R Sh 1992a *Russ. J. Inorganic Chem.* **37** 259

Pakhomov V I, Goryunov A V, Gladkii V V, Ivanova-Korfini I N and Kallaev S N 1992b *Russ. J. Inorganic Chem.* **37** 1447

Petrov V V, Khalakhnin A Yu, Pitsyga V G and Yachmenev V E 1988 *Sov. Phys.–Solid State* **30** 906

Petrov V V, Pitsyga V G, Gordeev V A, Bogdanova A V, Bagina M A and Khalakhnin A Yu 1983 *Sov. Phys.–Solid State* **25** 3465

Vlokh O G, Gribik V G, Kityk A V, Mokryi O M, Oleseyuk I D and Piroda S A 1990 *Crystallogr. Rep. (Kristallogr.)* **35** 1483

Werk M L, Chapuis G and Zuniga F J 1990 *Acta Crystallogr.* B **46** 187